Measurement of Cross Sections for b Jet Production in Events with a Z Boson in $p\overline{p}$ Collisions at $\sqrt{s} = 1.96$ TeV

T. Aaltonen,[24] J. Adelman,[14] T. Akimoto,[56] B. Álvarez González,[12] S. Amerio[w],[44] D. Amidei,[35] A. Anastassov,[39] A. Annovi,[20] J. Antos,[15] G. Apollinari,[18] A. Apresyan,[49] T. Arisawa,[58] A. Artikov,[16] W. Ashmanskas,[18] A. Attal,[4] A. Aurisano,[54] F. Azfar,[43] P. Azzurri[z],[47] W. Badgett,[18] A. Barbaro-Galtieri,[29] V.E. Barnes,[49] B.A. Barnett,[26] V. Bartsch,[31] G. Bauer,[33] P.-H. Beauchemin,[34] F. Bedeschi,[47] D. Beecher,[31] S. Behari,[26] G. Bellettini[x],[47] J. Bellinger,[60] D. Benjamin,[17] A. Beretvas,[18] J. Beringer,[29] A. Bhatti,[51] M. Binkley,[18] D. Bisello[w],[44] I. Bizjak[cc],[31] R.E. Blair,[2] C. Blocker,[7] B. Blumenfeld,[26] A. Bocci,[17] A. Bodek,[50] V. Boisvert,[50] G. Bolla,[49] D. Bortoletto,[49] J. Boudreau,[48] A. Boveia,[11] B. Brau[a],[11] A. Bridgeman,[25] L. Brigliadori,[44] C. Bromberg,[36] E. Brubaker,[14] J. Budagov,[16] H.S. Budd,[50] S. Budd,[25] S. Burke,[18] K. Burkett,[18] G. Busetto[w],[44] P. Bussey[k],[22] A. Buzatu,[34] K. L. Byrum,[2] S. Cabrera[u],[17] C. Calancha,[32] M. Campanelli,[36] M. Campbell,[35] F. Canelli,[18] A. Canepa,[46] B. Carls,[25] D. Carlsmith,[60] R. Carosi,[47] S. Carrillo[m],[19] S. Carron,[34] B. Casal,[12] M. Casarsa,[18] A. Castro[v],[6] P. Catastini[y],[47] D. Cauz[bb],[55] V. Cavaliere[y],[47] M. Cavalli-Sforza,[4] A. Cerri,[29] L. Cerrito[n],[31] S.H. Chang,[28] Y.C. Chen,[1] M. Chertok,[8] G. Chiarelli,[47] G. Chlachidze,[18] F. Chlebana,[18] K. Cho,[28] D. Chokheli,[16] J.P. Chou,[23] G. Choudalakis,[33] S.H. Chuang,[53] K. Chung,[13] W.H. Chung,[60] Y.S. Chung,[50] T. Chwalek,[27] C.I. Ciobanu,[45] M.A. Ciocci[y],[47] A. Clark,[21] D. Clark,[7] G. Compostella,[44] M.E. Convery,[18] J. Conway,[8] M. Cordelli,[20] G. Cortiana[w],[44] C.A. Cox,[8] D.J. Cox,[8] F. Crescioli[x],[47] C. Cuenca Almenar[u],[8] J. Cuevas[r],[12] R. Culbertson,[18] J.C. Cully,[35] D. Dagenhart,[18] M. Datta,[18] T. Davies,[22] P. de Barbaro,[50] S. De Cecco,[52] A. Deisher,[29] G. De Lorenzo,[4] M. Dell'Orso[x],[47] C. Deluca,[4] L. Demortier,[51] J. Deng,[17] M. Deninno,[6] P.F. Derwent,[18] G.P. di Giovanni,[45] C. Dionisi[aa],[52] B. Di Ruzza[bb],[55] J.R. Dittmann,[5] M. D'Onofrio,[4] S. Donati[x],[47] P. Dong,[9] J. Donini,[44] T. Dorigo,[44] S. Dube,[53] J. Efron,[40] A. Elagin,[54] R. Erbacher,[8] D. Errede,[25] S. Errede,[25] R. Eusebi,[18] H.C. Fang,[29] S. Farrington,[43] W.T. Fedorko,[14] R.G. Feild,[61] M. Feindt,[27] J.P. Fernandez,[32] C. Ferrazza[z],[47] R. Field,[19] G. Flanagan,[49] R. Forrest,[8] M.J. Frank,[5] M. Franklin,[23] J.C. Freeman,[18] I. Furic,[19] M. Gallinaro,[52] J. Galyardt,[13] F. Garberson,[11] J.E. Garcia,[21] A.F. Garfinkel,[49] K. Genser,[18] H. Gerberich,[25] D. Gerdes,[35] A. Gessler,[27] S. Giagu[aa],[52]

V. Giakoumopoulou,[3] P. Giannetti,[47] K. Gibson,[48] J.L. Gimmell,[50] C.M. Ginsburg,[18] N. Giokaris,[3] M. Giordani[bb],[55] P. Giromini,[20] M. Giunta[x],[47] G. Giurgiu,[26] V. Glagolev,[16] D. Glenzinski,[18] M. Gold,[38] N. Goldschmidt,[19] A. Golossanov,[18] G. Gomez,[12] G. Gomez-Ceballos,[33] M. Goncharov,[54] O. González,[32] I. Gorelov,[38] A.T. Goshaw,[17] K. Goulianos,[51] A. Gresele[w],[44] S. Grinstein,[23] C. Grosso-Pilcher,[14] R.C. Group,[18] U. Grundler,[25] J. Guimaraes da Costa,[23] Z. Gunay-Unalan,[36] C. Haber,[29] K. Hahn,[33] S.R. Hahn,[18] E. Halkiadakis,[53] B.-Y. Han,[50] J.Y. Han,[50] F. Happacher,[20] K. Hara,[56] D. Hare,[53] M. Hare,[57] S. Harper,[43] R.F. Harr,[59] R.M. Harris,[18] M. Hartz,[48] K. Hatakeyama,[51] C. Hays,[43] M. Heck,[27] A. Heijboer,[46] B. Heinemann,[29] J. Heinrich,[46] C. Henderson,[33] M. Herndon,[60] J. Heuser,[27] S. Hewamanage,[5] D. Hidas,[17] C.S. Hill[c],[11] D. Hirschbuehl,[27] A. Hocker,[18] S. Hou,[1] M. Houlden,[30] S.-C. Hsu,[29] B.T. Huffman,[43] R.E. Hughes,[40] U. Husemann,[36] M. Hussein,[36] U. Husemann,[61] J. Huston,[36] J. Incandela,[11] G. Introzzi,[47] M. Iori[aa],[52] A. Ivanov,[8] E. James,[18] B. Jayatilaka,[17] E.J. Jeon,[28] M.K. Jha,[6] S. Jindariani,[18] W. Johnson,[8] M. Jones,[49] K.K. Joo,[28] S.Y. Jun,[13] J.E. Jung,[28] T.R. Junk,[18] T. Kamon,[54] D. Kar,[19] P.E. Karchin,[59] Y. Kato,[42] R. Kephart,[18] J. Keung,[46] V. Khotilovich,[54] B. Kilminster,[18] D.H. Kim,[28] H.S. Kim,[28] H.W. Kim,[28] J.E. Kim,[28] M.J. Kim,[20] S.B. Kim,[28] S.H. Kim,[56] Y.K. Kim,[14] N. Kimura,[56] L. Kirsch,[7] S. Klimenko,[19] B. Knuteson,[33] B.R. Ko,[17] K. Kondo,[58] D.J. Kong,[28] J. Konigsberg,[19] A. Korytov,[19] A.V. Kotwal,[17] M. Kreps,[27] J. Kroll,[46] D. Krop,[14] N. Krumnack,[5] M. Kruse,[17] V. Krutelyov,[11] T. Kubo,[56] T. Kuhr,[27] N.P. Kulkarni,[59] M. Kurata,[56] S. Kwang,[14] A.T. Laasanen,[49] S. Lami,[47] S. Lammel,[18] M. Lancaster,[31] R.L. Lander,[8] K. Lannon[q],[40] A. Lath,[53] G. Latino[y],[47] I. Lazzizzera[w],[44] T. LeCompte,[2] E. Lee,[54] H.S. Lee,[14] S.W. Lee[t],[54] S. Leone,[47] J.D. Lewis,[18] C.-S. Lin,[29] J. Linacre,[43] M. Lindgren,[18] E. Lipeles,[46] A. Lister,[8] D.O. Litvintsev,[18] C. Liu,[48] T. Liu,[18] N.S. Lockyer,[46] A. Loginov,[61] M. Loreti[w],[44] L. Lovas,[15] D. Lucchesi[w],[44] C. Luci[aa],[52] J. Lueck,[27] P. Lujan,[29] P. Lukens,[18] G. Lungu,[51] L. Lyons,[43] J. Lys,[29] R. Lysak,[15] D. MacQueen,[34] R. Madrak,[18] K. Maeshima,[18] K. Makhoul,[33] T. Maki,[24] P. Maksimovic,[26] S. Malde,[43] S. Malik,[31] G. Manca[e],[30] A. Manousakis-Katsikakis,[3] F. Margaroli,[49] C. Marino,[27] C.P. Marino,[25] A. Martin,[61] V. Martin[l],[22] M. Martínez,[4] R. Martínez-Ballarín,[32] T. Maruyama,[56] P. Mastrandrea,[52] T. Masubuchi,[56] M. Mathis,[26] M.E. Mattson,[59] P. Mazzanti,[6]

K.S. McFarland,[50] P. McIntyre,[54] R. McNulty[j],[30] A. Mehta,[30] P. Mehtala,[24] A. Menzione,[47] P. Merkel,[49] C. Mesropian,[51] T. Miao,[18] N. Miladinovic,[7] R. Miller,[36] C. Mills,[23] M. Milnik,[27] A. Mitra,[1] G. Mitselmakher,[19] H. Miyake,[56] N. Moggi,[6] C.S. Moon,[28] R. Moore,[18] M.J. Morello[x],[47] J. Morlok,[27] P. Movilla Fernandez,[18] J. Mülmenstädt,[29] A. Mukherjee,[18] Th. Muller,[27] R. Mumford,[26] P. Murat,[18] M. Mussini[v],[6] J. Nachtman,[18] Y. Nagai,[56] A. Nagano,[56] J. Naganoma,[56] K. Nakamura,[56] I. Nakano,[41] A. Napier,[57] V. Necula,[17] J. Nett,[60] C. Neu[v],[46] M.S. Neubauer,[25] S. Neubauer,[27] J. Nielsen[g],[29] L. Nodulman,[2] M. Norman,[10] O. Norniella,[25] E. Nurse,[31] L. Oakes,[43] S.H. Oh,[17] Y.D. Oh,[28] I. Oksuzian,[19] T. Okusawa,[42] R. Orava,[24] S. Pagan Griso[w],[44] E. Palencia,[18] V. Papadimitriou,[18] A. Papaikonomou,[27] A.A. Paramonov,[14] B. Parks,[40] S. Pashapour,[34] J. Patrick,[18] G. Pauletta[bb],[55] M. Paulini,[13] C. Paus,[33] T. Peiffer,[27] D.E. Pellett,[8] A. Penzo,[55] T.J. Phillips,[17] G. Piacentino,[47] E. Pianori,[46] L. Pinera,[19] K. Pitts,[25] C. Plager,[9] L. Pondrom,[60] O. Poukhov*,[16] N. Pounder,[43] F. Prakoshyn,[16] A. Pronko,[18] J. Proudfoot,[2] F. Ptohos[i],[18] E. Pueschel,[13] G. Punzi[x],[47] J. Pursley,[60] J. Rademacker[c],[43] A. Rahaman,[48] V. Ramakrishnan,[60] N. Ranjan,[49] I. Redondo,[32] P. Renton,[43] M. Renz,[27] M. Rescigno,[52] S. Richter,[27] F. Rimondi[v],[6] L. Ristori,[47] A. Robson,[22] T. Rodrigo,[12] T. Rodriguez,[46] E. Rogers,[25] S. Rolli,[57] R. Roser,[18] M. Rossi,[55] R. Rossin,[11] P. Roy,[34] A. Ruiz,[12] J. Russ,[13] V. Rusu,[18] A. Safonov,[54] W.K. Sakumoto,[50] O. Saltó,[4] L. Santi[bb],[55] S. Sarkar[aa],[52] L. Sartori,[47] K. Sato,[18] A. Savoy-Navarro,[45] P. Schlabach,[18] A. Schmidt,[27] E.E. Schmidt,[18] M.A. Schmidt,[14] M.P. Schmidt*,[61] M. Schmitt,[39] T. Schwarz,[8] L. Scodellaro,[12] A. Scribano[y],[47] F. Scuri,[47] A. Sedov,[49] S. Seidel,[38] Y. Seiya,[42] A. Semenov,[16] L. Sexton-Kennedy,[18] F. Sforza,[47] A. Sfyrla,[25] S.Z. Shalhout,[59] T. Shears,[30] P.F. Shepard,[48] M. Shimojima[p],[56] S. Shiraishi,[14] M. Shochet,[14] Y. Shon,[60] I. Shreyber,[37] A. Sidoti,[47] P. Sinervo,[34] A. Sisakyan,[16] A.J. Slaughter,[18] J. Slaunwhite,[40] K. Sliwa,[57] J.R. Smith,[8] F.D. Snider,[18] R. Snihur,[34] A. Soha,[8] S. Somalwar,[53] V. Sorin,[36] J. Spalding,[18] T. Spreitzer,[34] P. Squillacioti[y],[47] M. Stanitzki,[61] R. St. Denis,[22] B. Stelzer,[34] O. Stelzer-Chilton,[34] D. Stentz,[39] J. Strologas,[38] G.L. Strycker,[35] D. Stuart,[11] J.S. Suh,[28] A. Sukhanov,[19] I. Suslov,[16] T. Suzuki,[56] A. Taffard[f],[25] R. Takashima,[41] Y. Takeuchi,[56] R. Tanaka,[41] M. Tecchio,[35] P.K. Teng,[1] K. Terashi,[51] J. Thom[h],[18] A.S. Thompson,[22]

* Deceased

G.A. Thompson,[25] E. Thomson,[46] P. Tipton,[61] P. Ttito-Guzmán,[32] S. Tkaczyk,[18] D. Toback,[54] S. Tokar,[15] K. Tollefson,[36] T. Tomura,[56] D. Tonelli,[18] S. Torre,[20] D. Torretta,[18] P. Totaro[bb],[55] S. Tourneur,[45] M. Trovato,[47] S.-Y. Tsai,[1] Y. Tu,[46] N. Turini[y],[47] F. Ukegawa,[56] S. Vallecorsa,[21] N. van Remortel[b],[24] A. Varganov,[35] E. Vataga[z],[47] F. Vázquez[m],[19] G. Velev,[18] C. Vellidis,[3] V. Veszpremi,[49] M. Vidal,[32] R. Vidal,[18] I. Vila,[12] R. Vilar,[12] T. Vine,[31] M. Vogel,[38] I. Volobouev[t],[29] G. Volpi[x],[47] P. Wagner,[46] R.G. Wagner,[2] R.L. Wagner,[18] W. Wagner,[27] J. Wagner-Kuhr,[27] T. Wakisaka,[42] R. Wallny,[9] S.M. Wang,[1] A. Warburton,[34] D. Waters,[31] M. Weinberger,[54] J. Weinelt,[27] W.C. Wester III,[18] B. Whitehouse,[57] D. Whiteson[f],[46] A.B. Wicklund,[2] E. Wicklund,[18] S. Wilbur,[14] G. Williams,[34] H.H. Williams,[46] P. Wilson,[18] B.L. Winer,[40] P. Wittich[h],[18] S. Wolbers,[18] C. Wolfe,[14] T. Wright,[35] X. Wu,[21] F. Würthwein,[10] S.M. Wynne,[30] S. Xie,[33] A. Yagil,[10] K. Yamamoto,[42] J. Yamaoka,[53] U.K. Yang[o],[14] Y.C. Yang,[28] W.M. Yao,[29] G.P. Yeh,[18] J. Yoh,[18] K. Yorita,[58] T. Yoshida,[42] G.B. Yu,[50] I. Yu,[28] S.S. Yu,[18] J.C. Yun,[18] L. Zanello[aa],[52] A. Zanetti,[55] X. Zhang,[25] Y. Zheng[d],[9] and S. Zucchelli[v],[6]

(CDF Collaboration[†])

[1]*Institute of Physics, Academia Sinica, Taipei, Taiwan 11529, Republic of China*

[2]*Argonne National Laboratory, Argonne, Illinois 60439*

[3]*University of Athens, 157 71 Athens, Greece*

[4]*Institut de Fisica d'Altes Energies,*

[†] With visitors from [a]University of Massachusetts Amherst, Amherst, Massachusetts 01003, [b]Universiteit Antwerpen, B-2610 Antwerp, Belgium, [c]University of Bristol, Bristol BS8 1TL, United Kingdom, [d]Chinese Academy of Sciences, Beijing 100864, China, [e]Istituto Nazionale di Fisica Nucleare, Sezione di Cagliari, 09042 Monserrato (Cagliari), Italy, [f]University of California Irvine, Irvine, CA 92697, [g]University of California Santa Cruz, Santa Cruz, CA 95064, [h]Cornell University, Ithaca, NY 14853, [i]University of Cyprus, Nicosia CY-1678, Cyprus, [j]University College Dublin, Dublin 4, Ireland, [k]Royal Society of Edinburgh/Scottish Executive Support Research Fellow, [l]University of Edinburgh, Edinburgh EH9 3JZ, United Kingdom, [m]Universidad Iberoamericana, Mexico D.F., Mexico, [n]Queen Mary, University of London, London, E1 4NS, England, [o]University of Manchester, Manchester M13 9PL, England, [p]Nagasaki Institute of Applied Science, Nagasaki, Japan, [q]University of Notre Dame, Notre Dame, IN 46556, [r]University de Oviedo, E-33007 Oviedo, Spain, [s]Texas Tech University, Lubbock, TX 79409, [t]IFIC(CSIC-Universitat de Valencia), 46071 Valencia, Spain, [u]University of Virginia, Charlottesville, VA 22904, [cc]On leave from J. Stefan Institute, Ljubljana, Slovenia,

Universitat Autonoma de Barcelona,
E-08193, Bellaterra (Barcelona), Spain
[5]*Baylor University, Waco, Texas 76798*
[6]*Istituto Nazionale di Fisica Nucleare Bologna,*
[v]*University of Bologna, I-40127 Bologna, Italy*
[7]*Brandeis University, Waltham, Massachusetts 02254*
[8]*University of California, Davis, Davis, California 95616*
[9]*University of California, Los Angeles, Los Angeles, California 90024*
[10]*University of California, San Diego, La Jolla, California 92093*
[11]*University of California, Santa Barbara, Santa Barbara, California 93106*
[12]*Instituto de Fisica de Cantabria, CSIC-University of Cantabria, 39005 Santander, Spain*
[13]*Carnegie Mellon University, Pittsburgh, PA 15213*
[14]*Enrico Fermi Institute, University of Chicago, Chicago, Illinois 60637*
[15]*Comenius University, 842 48 Bratislava,*
Slovakia; Institute of Experimental Physics, 040 01 Kosice, Slovakia
[16]*Joint Institute for Nuclear Research, RU-141980 Dubna, Russia*
[17]*Duke University, Durham, North Carolina 27708*
[18]*Fermi National Accelerator Laboratory, Batavia, Illinois 60510*
[19]*University of Florida, Gainesville, Florida 32611*
[20]*Laboratori Nazionali di Frascati, Istituto Nazionale*
di Fisica Nucleare, I-00044 Frascati, Italy
[21]*University of Geneva, CH-1211 Geneva 4, Switzerland*
[22]*Glasgow University, Glasgow G12 8QQ, United Kingdom*
[23]*Harvard University, Cambridge, Massachusetts 02138*
[24]*Division of High Energy Physics, Department of Physics,*
University of Helsinki and Helsinki Institute of Physics, FIN-00014, Helsinki, Finland
[25]*University of Illinois, Urbana, Illinois 61801*
[26]*The Johns Hopkins University, Baltimore, Maryland 21218*
[27]*Institut für Experimentelle Kernphysik,*
Universität Karlsruhe, 76128 Karlsruhe, Germany
[28]*Center for High Energy Physics: Kyungpook National University,*
Daegu 702-701, Korea; Seoul National University, Seoul 151-742,

Korea; Sungkyunkwan University, Suwon 440-746,
Korea; Korea Institute of Science and Technology Information, Daejeon,
305-806, Korea; Chonnam National University, Gwangju, 500-757, Korea
[29]*Ernest Orlando Lawrence Berkeley National Laboratory, Berkeley, California 94720*
[30]*University of Liverpool, Liverpool L69 7ZE, United Kingdom*
[31]*University College London, London WC1E 6BT, United Kingdom*
[32]*Centro de Investigaciones Energeticas*
Medioambientales y Tecnologicas, E-28040 Madrid, Spain
[33]*Massachusetts Institute of Technology, Cambridge, Massachusetts 02139*
[34]*Institute of Particle Physics: McGill University, Montréal,*
Québec, Canada H3A 2T8; Simon Fraser University, Burnaby,
British Columbia, Canada V5A 1S6; University of Toronto,
Toronto, Ontario, Canada M5S 1A7; and TRIUMF,
Vancouver, British Columbia, Canada V6T 2A3
[35]*University of Michigan, Ann Arbor, Michigan 48109*
[36]*Michigan State University, East Lansing, Michigan 48824*
[37]*Institution for Theoretical and Experimental Physics, ITEP, Moscow 117259, Russia*
[38]*University of New Mexico, Albuquerque, New Mexico 87131*
[39]*Northwestern University, Evanston, Illinois 60208*
[40]*The Ohio State University, Columbus, Ohio 43210*
[41]*Okayama University, Okayama 700-8530, Japan*
[42]*Osaka City University, Osaka 588, Japan*
[43]*University of Oxford, Oxford OX1 3RH, United Kingdom*
[44]*Istituto Nazionale di Fisica Nucleare, Sezione di Padova-Trento,*
[w]*University of Padova, I-35131 Padova, Italy*
[45]*LPNHE, Universite Pierre et Marie*
Curie/IN2P3-CNRS, UMR7585, Paris, F-75252 France
[46]*University of Pennsylvania, Philadelphia, Pennsylvania 19104*
[47]*Istituto Nazionale di Fisica Nucleare Pisa,* [x]*University of Pisa,*
[y]*University of Siena and* [z]*Scuola Normale Superiore, I-56127 Pisa, Italy*
[48]*University of Pittsburgh, Pittsburgh, Pennsylvania 15260*
[49]*Purdue University, West Lafayette, Indiana 47907*

[50] University of Rochester, Rochester, New York 14627
[51] The Rockefeller University, New York, New York 10021
[52] Istituto Nazionale di Fisica Nucleare, Sezione di Roma 1,
[aa] Sapienza Università di Roma, I-00185 Roma, Italy
[53] Rutgers University, Piscataway, New Jersey 08855
[54] Texas A&M University, College Station, Texas 77843
[55] Istituto Nazionale di Fisica Nucleare Trieste/Udine,
[bb] University of Trieste/Udine, Italy
[56] University of Tsukuba, Tsukuba, Ibaraki 305, Japan
[57] Tufts University, Medford, Massachusetts 02155
[58] Waseda University, Tokyo 169, Japan
[59] Wayne State University, Detroit, Michigan 48201
[60] University of Wisconsin, Madison, Wisconsin 53706
[61] Yale University, New Haven, Connecticut 06520

Abstract

A measurement of the b jet production cross section is presented for events containing a Z boson produced in $p\bar{p}$ collisions at $\sqrt{s} = 1.96$ TeV, using data corresponding to an integrated luminosity of 2 fb^{-1} collected by the CDF II detector at the Tevatron. Z bosons are selected in the electron and muon decay modes. Jets are considered with transverse energy $E_T > 20$ GeV and pseudorapidity $|\eta| < 1.5$ and are identified as b jets using a secondary vertex algorithm. The ratio of the integrated Z+b jet cross section to the inclusive Z production cross section is measured to be $3.32 \pm 0.53(\text{stat.}) \pm 0.42(\text{syst.}) \times 10^{-3}$. This ratio is also measured differentially in jet E_T, jet η, Z-boson transverse momentum, number of jets, and number of b jets. The predictions from leading order Monte Carlo generators and next-to-leading-order QCD calculations are found to be consistent with the measurements within experimental and theoretical uncertainties.

PACS numbers:

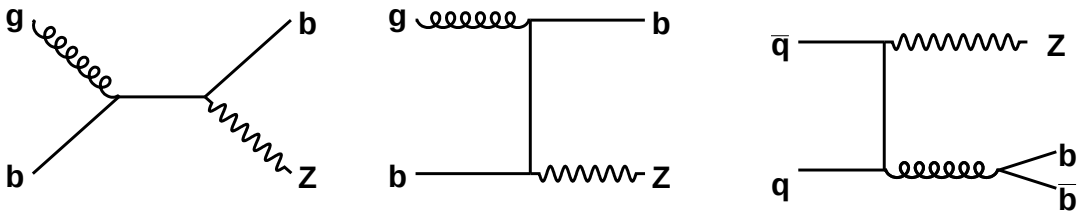

FIG. 1: Leading order Feynman diagrams for $gb \to Zb$ and $q\bar{q} \to Zb\bar{b}$ production.

I. INTRODUCTION

The associated production of Z bosons and one or more b jets provides an important test of quantum-chromodynamics (QCD) calculations, for which the theoretical predictions for this process vary significantly [1–3]. The understanding of this process and its description by current theoretical calculations is important since it is the largest background, e.g., to the search for the standard model Higgs boson in the $ZH \to Zb\bar{b}$ decay mode [4] and to searches for the supersymmetric partners of b quarks [5, 6]. The process is also sensitive to the b quark density in the proton. A precise knowledge of the b quark density is necessary to accurately predict processes that strongly depend on it such as electroweak production of single top quarks [7] or the production of Higgs bosons within certain supersymmetric models [8, 9].

The Feynman diagrams of the contributing leading order processes $gb \to Zb$ and $q\bar{q} \to Zb\bar{b}$ are shown in Fig. 1. In the first two diagrams a b quark from the proton undergoes a hard scatter and a $\bar{b}$ quark typically remains close to the parent proton and may not be detected. In the third diagram the $b\bar{b}$ quark pair can be produced close to each other and may sometimes be reconstructed in the same jet (referred to as a "$b\bar{b}$ jet"). According to QCD calculations the latter diagram is predicted to account for approximately 50% of b jet production in association with a Z boson at the Tevatron [1].

Previously the integrated cross section for $Z + b$ jet production has been measured with an uncertainty of 39% by the CDF collaboration [10]. The D0 collaboration also measured this process assuming the ratio of the $Z + b$ jet to $Z + c$ jet cross section from next-to-leading order (NLO) QCD calculations [11]. The cross section of Z+jets production has also been measured recently by both collaborations and found to agree well with QCD

calculations [12, 13]. A preliminary measurement has been made of the related $W + b$ jet process[14].

In this article we present an update to the integrated $Z + b$ jet cross section measurement with a substantially reduced uncertainty and for the first time differential cross section measurements. The measurement is made by selecting pairs of electrons or muons (dileptons) with an invariant mass consistent with the mass of the Z boson, M_Z, and jets containing a displaced secondary vertex consistent with the decay of a bottom hadron. Contributions from the decay of known heavy particles (such as Z or top quarks) to b hadrons are not included in our definition of the cross section and are subtracted from the data.

The light and charm jets (i.e., jets that do not contain a b hadron) remaining after this selection are discriminated from b jets using the invariant mass of all charged particles associated to the secondary vertex, exploiting the large mass of the b quark compared to the other partons. Throughout this article we use Z to denote any dilepton events due to Z or γ^* production with an invariant mass $76 < M_{ll} < 106$ GeV/c^2, albeit the contribution of virtual photons is predicted to be below 1% of the Z production rate [15].

We use data collected by the CDF II detector at the Tevatron $p\bar{p}$ collider between February 2002 and May 2007, corresponding to an integrated luminosity of 2.0 fb^{-1}.

II. THE CDF II DETECTOR

The CDF II detector is described in detail elsewhere [16] and consists of a precision tracking system, electromagnetic and hadronic calorimeters and muon spectrometers. The tracking detector is coaxial with the beam-pipe and consists of silicon strip detectors [17] surrounded by a wire drift chamber (COT) [18] inside a 1.4 T magnetic field provided by a solenoid. The solenoid is surrounded by electromagnetic [19, 20] and hadronic calorimeters [21] that use lead and stainless steel as absorber materials, respectively, and scintillators as active material. Inside the electromagnetic calorimeter a proportional strip and wire chamber is embedded at about 6 radiation lengths, providing an accurate position measurement [22]. The muon detectors [23] surround the calorimeters and consist of wire chambers and scintillators. Gas Čerenkov counters, located close to the beampipe, are used to measure a fraction of the inelastic event rate and thereby the collider luminosity [24].

A cylindrical coordinate system is used in which the z axis is along the proton beam

direction and θ is the polar angle. The pseudorapidity is defined as $\eta = -\ln\tan(\theta/2)$, while the transverse momentum is given by $p_T = p\sin\theta$ and the transverse energy by $E_T = E\sin\theta$. Missing transverse energy, $\not\!\!E_T$, is defined as the magnitude of $-\Sigma_i E_T^i \hat{n}_i$, where E_T^i is the transverse energy deposited in the i^{th} calorimeter tower and $\hat{n}_i$ is a unit vector pointing from the beamline to the ith tower in the azimuthal plane.

III. MEASUREMENT PROCEDURE

In this article we present a measurement of the ratio of the cross section for $Z + b\,\text{jet}$ production to the inclusive Z production cross section. Measuring the ratio has the advantage that several uncertainties, e.g., on the integrated luminosity and on the lepton identification, largely cancel. We present both per jet and per event cross section ratios. The per jet cross section ratio is proportional to the number of b jets, while the per event cross section ratio is proportional to the number of events with one or more b jets. The per jet cross section selection efficiency is independent of the number of b jets in the event as it is proportional directly to the efficiency of identifying a b jet, $\epsilon_{b\,\text{jet}}$, and thus has a smaller overall error. For certain measurements, such as the cross section ratio as a function of the number of jets, it is preferable to use an event based definition. In this case the event selection efficiency depends on the number of b jets in the event: for events with one b jet it is also simply proportional to $\epsilon_{b\,\text{jet}}$ while for events with two b jets the efficiency for, e.g., identifying at least one b jet is proportional to $\epsilon_{b\,\text{jet}} \cdot (2 - \epsilon_{b\,\text{jet}})$.

The cross section ratios are determined by

$$\frac{\sigma^{\text{jet}}(Z + b\,\text{jet})}{\sigma(Z)} = \frac{N^{\text{jet}}(Z + b\,\text{jet})/N(Z)}{\epsilon^{\text{jet}}(Z + b\,\text{jet})/\epsilon(Z)} \quad (1)$$

$$\frac{\sigma^{\text{evt}}(Z + N_{b\,\text{jet}})}{\sigma(Z)} = \frac{N^{\text{evt}}(Z + N_{b\,\text{jet}})/N(Z)}{\epsilon^{\text{evt}}(Z + N_{b\,\text{jet}})/\epsilon(Z)}, \quad (2)$$

where $N(Z)$ is the number of events in the data with a Z boson and $\epsilon(Z)$ is the efficiency $\times$ acceptance for the Z boson selection within the M_{ll} range of this analysis. For the per jet cross sections, $\sigma^{\text{jet}}(Z + b\,\text{jet})$, the number of estimated b jets in data for events with a Z boson is $N^{\text{jet}}(Z + b\,\text{jet})$. For the per event cross sections, $\sigma^{\text{evt}}(Z + N_{b\,\text{jet}})$, the number of data events with a Z boson is $N^{\text{evt}}(Z + N_{b\,\text{jet}})$, with each event having the number of b jets equal to $N_{b\,\text{jet}}$. All quantities are quoted after background subtraction. The quantities $\epsilon^{\text{jet}}(Z + b\,\text{jet})$

and $\epsilon^{\rm evt}(Z + N_{b\,\rm jet})$ are the corresponding efficiency $\times$ acceptances for the $Z + b$ jet and the $Z + N_{b\,\rm jet}$ selections, respectively.

In the following, the selection and the methods for determining the efficiencies and the number of b jets are described. The Monte Carlo simulation is tuned to reproduce the trigger, lepton, and b jet efficiencies as measured in the data, and is used to correct the data for all detector effects such as acceptance losses, efficiencies and resolutions.

IV. MONTE CARLO SIMULATION

We use PYTHIA [2] and ALPGEN [3] as the main Monte Carlo generators. For the PYTHIA generation the inclusive Drell-Yan process for Z production is used, and jets are generated via the parton shower. This process includes matrix-element inspired corrections to the parton shower to better describe the p_T distribution of the Z boson [25]. ALPGEN calculates the leading order (LO) matrix elements separately for each parton emission and then matches to a parton shower from PYTHIA. Double-counting between the matrix-element calculations and the parton-showers is avoided by using the MLM matching procedure [26]. For both PYTHIA and ALPGEN the CTEQ5L [27] structure function is used for the parton distribution functions and "Tune A" is used for the underlying event [28, 29]. For the modeling of c and b jets a combination of PYTHIA and ALPGEN is used: the samples are averaged using equal portions of both since this gives the best description of the E_T and η distribution of the b jets. For the description of light jets we use only the PYTHIA sample which gives a good description of inclusive Z+jet production at low jet multiplicities that are relevant for this analysis. The decays of b hadrons are performed using EVTGEN [30]. The generated events are passed through the GEANT3-based [31] CDF detector simulation [32], and thereafter reconstructed and analyzed in the same way as the data.

V. EVENT SELECTION

Z boson candidates are identified in events with a dilepton pair which have an invariant mass M_{ll} between 76 and 106 GeV/c^2 where $\ell = e, \mu$.

Events in the electron channel are triggered online by either one central ($|\eta| < 1.1$) electromagnetic calorimeter cluster with $E_T > 18$ GeV and a track with $p_T > 9$ GeV/c

associated to it, or by two electromagnetic clusters with $E_T > 18$ GeV and $|\eta| < 3.2$, where no track association is required. These requirements are also made in the offline analysis. Furthermore, all central electrons are required to have $E_T > 10$ GeV and a matched track with $p_T > 5$ GeV/c, and all forward electrons are required to have $E_T > 18$ GeV. For forward electrons ($1.1 < |\eta| < 3.2$) a track requirement is not imposed unless both electrons are forward, in which case they are required to have $E_T > 25$ GeV and a matched track with $p_T > 10$ GeV/c. The electrons also have to pass certain quality criteria to verify that they are consistent with the electromagnetic shower characteristics expected for electrons [15].

Events in the muon channel are triggered on at least one muon candidate that has a signal in one of the muon chambers with $|\eta| < 1.0$ and $p_T > 18$ GeV/c. In the offline analysis the second muon candidate is not required to have a signal in the muon chambers but it must have hits in the COT which reduces the acceptance to $|\eta| \lesssim 1.5$. All muons are required to have calorimeter energy deposits consistent with those expected from a minimum ionizing particle [15].

All leptons are required to be isolated from other particles in the event by a distance of $\Delta R = \sqrt{(\Delta\phi)^2 + (\Delta\eta)^2} > 0.4$, and at least one of the two muons (electrons) must have $p_T > 18$ GeV/c ($E_T > 18$ GeV) while the second one is only required to have $p_T > 10$ GeV/c ($E_T > 10$ GeV). However, for dielectron events where the two electrons are in the forward calorimeter, both are required to have $E_T > 18$ GeV to match the trigger requirements.

In order to reduce the background from particles that fake electrons or muons the two leptons in each event are required to have opposite charge. This cut is not applied in the electron channel if one or both electrons are forward, since the charge determination is not very precise in this region of the detector [33].

Using this selection we observe 193,749 $Z \to e^+e^-$ and 101,967 $Z \to \mu^+\mu^-$ candidates. The selection has $\epsilon(Z) = 41\%$ for $Z \to e^+e^-$ and $\epsilon(Z) = 23\%$ for $Z \to \mu^+\mu^-$ events.

Jets are selected using a cone based algorithm with a cone size of $\Delta R = 0.7$ [34]. This choice of cone size has the advantage over smaller cone sizes in that the hadronization corrections are smaller. The jets are measured in the calorimeter and corrected to the hadron level [35], i.e., they are corrected for the CDF calorimeter response and multiple $p\bar{p}$ interactions. Note that the jets are not corrected for the underlying event (underlying event correction) or any changes in the energy contained within the jet cone due to fragmentation and any energy loss due to out-of-cone parton radiation (hadronization correction). In order

to compare to parton level calculations, these additional corrections are determined and applied to the theoretical calculation as described later. We observe 29,363 $Z \to e^+e^-$ and 18,087 $Z \to \mu^+\mu^-$ candidate events with at least one jet with $E_T > 20$ GeV and $|\eta| < 1.5$.

A b jet is defined at the hadron level as any jet that contains a b hadron within its cone. A secondary vertex algorithm is used to identify b jets based on tracks with $p_T > 0.5$ GeV/c that are displaced from the primary vertex, exploiting the relatively long lifetime of b hadrons, as described in detail in Ref. [36]. Jets with a reconstructed secondary vertex are denoted as "tagged" jets. The b tagging efficiency varies between 30% and 40% in the E_T range relevant for this analysis, and has been measured using data with an uncertainty of 5.3%. The algorithm also tags about 8% of c jets and 0.5% of light jets as determined with Monte Carlo simulation.

A sign is assigned depending on whether the secondary vertex is in the same hemisphere as the jet (positive tag) or in the opposite hemisphere (negative tag). For b jets the direction of the vertex tag is aligned with the jet direction generally yielding a positive tag, while for misreconstructed secondary vertices from light jets the two directions are uncorrelated, yielding similar amounts of negative and positive tags. Since the jets with negative tags are used in the fit to determine the fraction of b jets (see section VII), it is necessary to verify that the ratio of negatively to positively tagged light jets in the Monte Carlo reproduces that in the data. The ratio has been measured in inclusive jet production as 0.65 ± 0.07, in good agreement with the simulation value of 0.62.

Events are rejected if $\not\!\!E_T > 25$ GeV and the sum of the transverse energies of all jets, leptons and $\not\!\!E_T$ is greater than 150 GeV. These cuts reduce the background from $t\bar{t}$ production by a factor 10, while retaining 99% of the signal.

The efficiency of this selection is $\epsilon^{\rm jet}(Z + b\,{\rm jet}) = 8.7\%$. In the data we observe 648 positively tagged jets and 151 negatively tagged jets. There are nine events that contain two tagged jets. For these events all tags are found to be positive.

The sample of tagged events contains a small amount of background from known processes which have a true b jet and a larger background contribution from events where a c jet or a light jet has produced a secondary vertex tag. These backgrounds are discussed in the next two sections.

VI. BACKGROUND CONTRIBUTIONS

The most important backgrounds that contain a true b jet arise from ZZ and $t\bar{t}$ production and from processes where one or two jets are misidentified as a lepton. This latter contribution arises mainly from W+jets events where one jet is misidentified and multi-jet production where two jets are misidentified. Background from non-b jets is discussed in section VII.

The ZZ and $t\bar{t}$ backgrounds are determined using PYTHIA Monte Carlo simulation. The ZZ Monte Carlo simulation is normalized to the NLO QCD cross section calculation of 37.2 fb [37], which is the part of the cross section where both Zs are in the mass range $76 < M_Z < 106$ GeV/c^2 and where one Z decays to any of the charged leptons and the other to $b\bar{b}$. The Monte Carlo simulation also produces events for γ^*/Z production outside this mass range and for all standard model decays. The $t\bar{t}$ cross section is taken from NLO QCD as 6.7 pb [38]. We estimate an uncertainty on these backgrounds of 20%, which takes into account the uncertainty in the theoretical prediction for the production cross section and in the experimental acceptance for our analysis. Backgrounds from $Z \to \tau^+\tau^-$ and WW production were also studied. Both were found to be small, with $Z \to \tau^+\tau^-$ contributing 0.3 and WW contributing < 0.01 to the number of tagged jets.

The backgrounds due to jets being misidentified as leptons are determined using the data. For the dielectron channel a "fake rate" method is used where the fraction of jets misidentified as electrons is measured in inclusive jet samples and then applied to the jets in a sample of data events with one reconstructed electron. This technique is described in more detail in Refs. [10] and [39]. The uncertainty on this background is estimated at 50%, using the agreement between data and Monte Carlo simulation in the sidebands of the Z mass distribution. For the dimuon channel we use events in which both muons have the same electric charge since the chance of faking a muon is assumed to be charge independent. The statistical error on this number of events is used as the uncertainty. The resulting background estimates for the number of tagged jets (including both positive and negative tags) are shown in Table I.

The dilepton invariant mass is shown in Fig. 2 for events with at least one positively tagged jet for the data, the PYTHIA signal Monte Carlo sample, and the background processes. The signal Drell-Yan Monte Carlo sample is normalized such that the expectation equals the

TABLE I: Estimated numbers of background tagged jets (positive and negative) for the e^+e^- and the $\mu^+\mu^-$ channels. The uncertainties include both statistical and systematic errors.

Background source	e^+e^-	$\mu^+\mu^-$
ZZ	6.5 ± 1.3	4.3 ± 0.9
$t\bar{t}$	1.3 ± 0.3	1.4 ± 0.3
$Z \to \tau^+\tau^-$ / WW	0.2 ± 0.1	0.1 ± 0.1
fake lepton	16.4 ± 8.2	5.0 ± 2.2

number of data events in the range $76 < M_{ll} < 106$ GeV/c^2. The shape of expectation agrees well with the data distribution both in the peak, where the Drell-Yan signal dominates, and in the tails, where the background is significant.

VII. DETERMINATION OF THE FRACTION OF *b* JETS

After the selection described in section V the sample of tagged jets contains a significant fraction of light and charm jets. Since the $Z + c$ jet cross section in the data is unknown and the simulation may not accurately describe the rate of light jets that are reconstructed with a secondary vertex, the fraction of b jets in the data is determined using a likelihood fit of the invariant mass distribution of the tracks forming the secondary vertex M_{SVTX}. Due to the different masses of the quarks this distribution enables a good discrimination between light, c, and b jets. It should be noted that these distributions are affected, particularly for low values, by the minimum track p_T requirement and the efficiency of the algorithm to correctly assign tracks to the secondary vertex.

The fit is performed for $M_{SVTX} < 3.5$ GeV/c^2 where the data have reasonable statistics. The Z+jets Monte Carlo simulation and the simulation for the background processes, apart from fake leptons, are used to make templates for the shape of the M_{SVTX} distributions for light, c and b jets. The template for the shape of the background from fake leptons is taken from the data. The normalization of each background is fixed (see section VI), while the normalizations of the light, c, and b components of the Z+jets are free parameters of the fit.

This fit is done simultaneously for positively and negatively tagged jets. We include the negatively tagged jets in the fit since this results in a reduced uncertainty on the number of

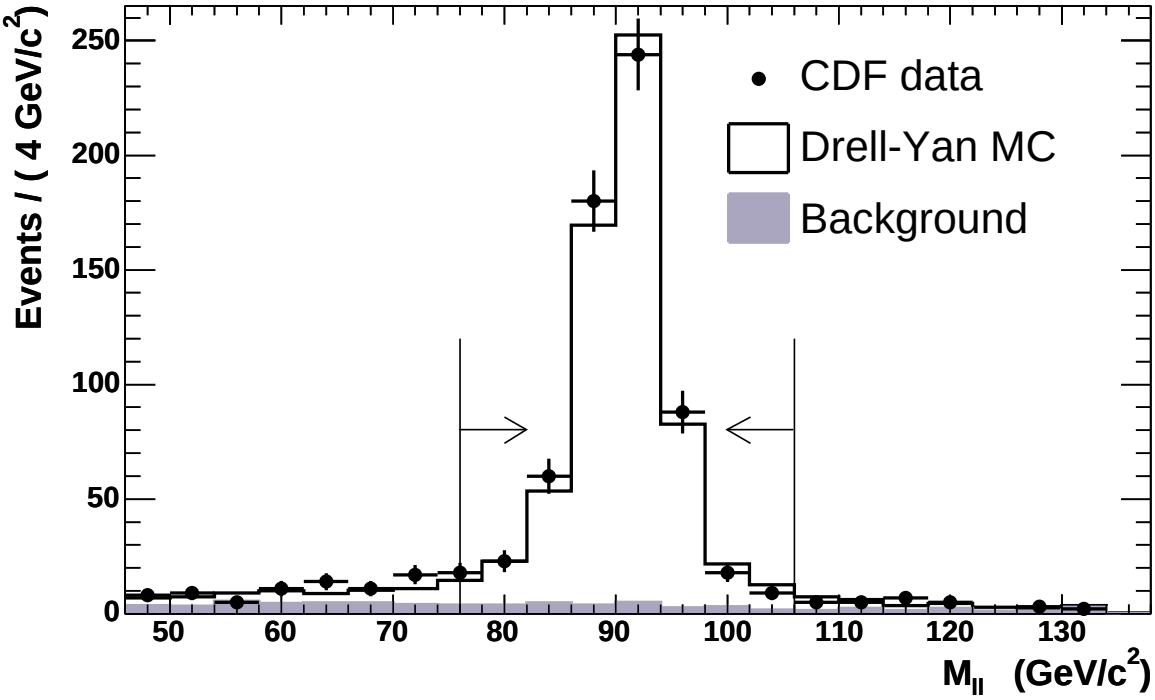

FIG. 2: Dilepton invariant mass for events with at least one positive secondary vertex tag. The data (points) are shown together with the Drell-Yan Monte Carlo (open histogram) and the sum of the background contributions (filled histogram). The range where the data are selected for this analysis is indicated by arrows.

light and c jets, although the effect on the uncertainty for the number of b jets is marginal. The resulting fit is shown in Fig. 3. It is seen that for the positively tagged jets the b jets populate the higher M_{SVTX} values due to the large b quark mass, allowing them to be discriminated from the light and charm background that is concentrated at low M_{SVTX}. The negatively tagged jets are mainly populated by light jets, which are thus constrained by including this distribution in the fit. The fit yields the number of positively tagged b jets as $N_b = 270 \pm 43$. The correlation coefficient between the number of b and c jets is -0.78 and between the number of b jets and light jets is $+0.22$. As a consistency check, when fitting only the positively tagged jets, the result of $N_b = 273 \pm 44$ is consistent with the default fit.

This technique for estimating the number of b jets is used for the integrated and all differential cross section measurements except for the $Z + 2b$ jets measurement for which the statistics are too low to use this fit procedure. Since the background for double-tagged events

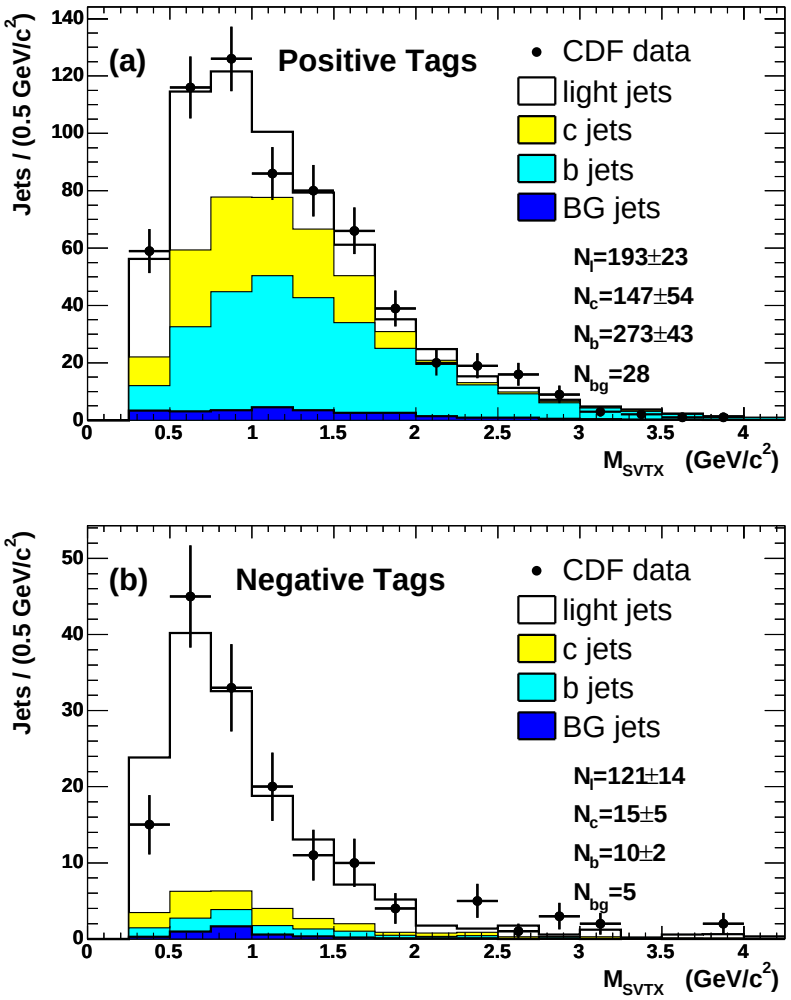

FIG. 3: Invariant mass of tracks at the secondary vertex for (a) positively and (b) negatively tagged jets. Shown are the data (points) and the fitted contributions of light, c and b jets. Also shown is the background contribution from Z+light jets, $Z + c$ jets, and from other processes with b jets. The fitted number of light jets (N_l), c jets (N_c), b jets (N_b), and the number of background events (N_{bg}) is also shown.

from c and light flavor jets is predicted from Monte Carlo to be only 0.79 events, compared to 9 observed data events we simply subtract those components using the prediction.

VIII. SYSTEMATIC UNCERTAINTIES

There are several sources of systematic uncertainty that are all evaluated separately for the integrated $Z + b$ jet cross section and for each bin of the differential measurements. Table II lists each source of systematic uncertainty and its effect on the integrated cross section ratio.

TABLE II: The systematic uncertainties on the measurement of the ratio $\sigma^{\rm jet}(Z + b\,{\rm jet})/\sigma(Z)$. The total systematic uncertainty is estimated by adding the individual uncertainties in quadrature.

Source of Uncertainty	Uncertainty (%)
MC $E_T^{\rm jet}$ dependence	8.0
MC $\eta^{\rm jet}$ dependence	2.8
track finding efficiency	5.7
b quark fragmentation	0.8
$b\bar{b}/b$, $c\bar{c}/c$ jet fractions	3.8
light jet template	1.7
b-tagging efficiency	5.3
jet energy scale	2.4
misidentified lepton background	1.9
other backgrounds	0.8
total	12.7

The largest systematic uncertainties arise from the Monte Carlo modeling of the b jet E_T distribution and the shape of the templates used for the extraction of the b jet fraction.

The uncertainty on the E_T dependence of b jets in $Z + b$ jet production is estimated directly from the data by reweighting the shape of the simulated distribution maintaining consistency with the data at the 1σ level. These variations are of a similar magnitude as the differences between the PYTHIA and ALPGEN generators. The resulting uncertainty is 8.0%. The same technique is used to estimate a systematic uncertainty due to the modeling of the jet η distribution of 2.8%.

Systematic uncertainties on the shape of the M_{SVTX} templates are estimated by varying the track finding efficiency by 3%, by changing the b quark fragmentation function, and

by varying the fraction of $b\bar{b}$ to b jets (and $c\bar{c}$ to c jets) between zero and three times their default values in the simulation. These result in cross section uncertainties of 5.7%, 0.8%, and 3.8%, respectively. For the light jet template the relative contribution of negative tags with respect to positive tags is varied by 25%, resulting in a cross section uncertainty of 1.7%. The b-tagging efficiency uncertainty of 5.3% results in an uncertainty on the cross sections with one b jet of 5.3% and on those with two b jets of 10.6%. Additional uncertainties arise from the jet energy scale [35] (2.4%) and the backgrounds as described in section VI (2.0%).

All these uncertainties apply to the ratio of the $Z + b$ jet to the Z cross section. For the $Z + b$ jet cross section itself, additional uncertainties apply due to the uncertainty on the integrated luminosity (5.8%) [40] and on the CDF measurement of the Z cross section (1.8%) [15].

While the per-jet cross section is independent of the Monte Carlo model used for the number of b jets in each event, the event based cross sections depend on the assumption on this number. We estimate a systematic uncertainty on the ratio of events with two b jets to one b jet of 30% as determined from the measurement of the cross section ratio for one and two b jets presented in section IX. This results in an additional uncertainty of up to 4.7% on any event based cross section.

For the measurement of $\sigma^{\rm evt}(Z + 2b\,{\rm jets})/\sigma(Z)$ an uncertainty of 100% on the c and light jet backgrounds is taken, resulting in an uncertainty of 12% on the cross section ratio.

IX. RESULTS

In this section the integrated and differential measurements for the $Z + b$ jet cross section divided by the inclusive Z cross section are presented. Also shown are the integrated cross section and the integrated cross section divided by the Z+jet cross section.

The measurements are compared to the leading-order QCD Monte Carlo generators PYTHIA and ALPGEN, and to the next-to-leading order calculations as implemented in MCFM [1]. The QCD calculations are always performed in the same kinematic range as the data.

The MCFM calculation is performed at order α_s^2. The $gb \to Zb$ is dependent on the b quark density, and is performed at next-to-leading order in α_s. The other processes contributing at order α_s^2 are the final states Zbg and $Zb\bar{b}$, which are calculated at leading order. The b

quarks are treated as massless throughout, except in the contribution $q\bar{q} \to Zb\bar{b}$ where the quark mass is required in order to render the calculation finite. The NLO corrections are known to substantially increase the cross section for the $gb \to Zb$ process and to decrease its dependence on renormalization and factorization scales. For the $q\bar{q} \to Zb\bar{b}$ process no full NLO calculations are available for the case where only one b jet is observed. This leads to a substantial uncertainty on the cross section as discussed below. For the results presented here two predictions are compared: $Q^2 = m_Z^2 + p_{T,Z}^2$ and $Q^2 = (\sum_{i=1}^{N_{\rm jet}} p_{T,i}^2)/N_{\rm jet} = \langle p_{T,\rm jet}^2 \rangle$. The same scales are used for the renormalization and factorization scale for the two predictions.

ALPGEN is a tree-level generator where the partonic initial and final states are showered using PYTHIA. In the evaluation of the matrix elements, ALPGEN treats b quarks as massive, and therefore b quarks cannot be considered as parts of the partonic density of the proton. The inclusive $Z + b$ final state emerges in ALPGEN as part of the full $gg \to Zb\bar{b}$ process after summing over the full phase-space of the $\bar{b}$ quark. The result is dominated by configurations where one of the initial-state gluons splits into a $b\bar{b}$ pair: here, the b quark enters the hard scattering with the second gluon leading to the $Z + b$ final state, and the $\bar{b}$ typically has small transverse momentum and large rapidity. For ALPGEN the default renormalization and factorization scales of $Q^2 = m_Z^2 + p_{T,Z}^2$ are used.

PYTHIA includes the $b\bar{b} \to Z$ process as part of the generic $q\bar{q} \to Z$ process, with a cross section related to the parton density of the incoming $b\bar{b}$ quarks evaluated at the Z mass scale. Then, by backwards evolution of the initial-state cascade, two branchings $g \to b\bar{b}$ are constructed to promote the original process to $gg \to Zb\bar{b}$, where the scale is set by the transverse momentum (in some approximation) of each branching on its own. In addition further partons may be emitted in the cascade, and one may also have light quark $q\bar{q} \to Z$ processes where final-state $g \to b\bar{b}$ branchings gives $Zb\bar{b}$ topologies.

For MCFM the CTEQ6M [41] parton distribution functions are used, while for PYTHIA and ALPGEN the CTEQ5L set is used.

Corrections for the underlying event and the hadronization (see section V) are determined using the PYTHIA Monte Carlo and applied to the MCFM prediction. The underlying event correction is determined by taking the difference in the cross section with and without the underlying event switched on. The hadronization correction is determined by taking the difference in the cross section at the parton and hadron level. For $\sigma^{\rm jet}(Z + b\,{\rm jet})/\sigma(Z)$ and the integrated $Z + b\,$jet cross section, these corrections result in a net increase of the

predicted cross section by 8% with contributions of -1% from hadronization and $+9\%$ from the underlying event. For the cross section ratio of $Z + b$ jet to inclusive Z+jet production the correction is $+4\%$ with contributions of $+9\%$ from hadronization and -5% from the underlying event. The correction factors for the differential cross section ratios are given below.

The ratio of the integrated $Z + b$ jet cross section for $E_T^{b\,\mathrm{jet}} > 20$ GeV and $|\eta^{b\,\mathrm{jet}}| < 1.5$ to inclusive Z production, for $76 < M_{ll} < 106$ GeV/c^2, is measured as

$$\frac{\sigma^{\mathrm{jet}}(Z + b\,\mathrm{jet})}{\sigma(Z)} = (3.32 \pm 0.53(\mathrm{stat.}) \pm 0.42(\mathrm{syst.})) \times 10^{-3}.$$

This measurement is proportional to the number of b jets. The NLO QCD prediction of MCFM is 2.3×10^{-3} for $Q^2 = m_Z^2 + p_{T,Z}^2$ and 2.8×10^{-3} for $Q^2 = \langle p_{T,\mathrm{jet}}^2 \rangle$. The prediction of ALPGEN is 2.1×10^{-3} and PYTHIA predicts 3.5×10^{-3}. The difference between the two MCFM predictions shows that there is a rather large theoretical uncertainty for this process. The reason for the large difference between ALPGEN and PYTHIA is primarily due to the use of different scales since ALPGEN uses a large scale while PYTHIA's scale is approximately the jet p_T. The data are better described by a low choice of scale.

The ratio of $Z + b$ jet to inclusive Z+jet production is determined as $(2.08 \pm 0.33 \pm 0.34)\%$ compared to predictions of 1.8% (MCFM, $Q^2 = m_Z^2 + p_{T,Z}^2$), 2.2% (MCFM, $Q^2 = \langle p_{T,\mathrm{jet}}^2 \rangle$), 1.5% (ALPGEN), and 2.2% (PYTHIA). The Z+b jet cross section is determined to be $\sigma^{\mathrm{jet}}(Z$+$b\,\mathrm{jet}) = 0.85 \pm 0.14(\mathrm{stat.}) \pm 0.12(\mathrm{syst.})$ pb by multiplying the ratio with the measured inclusive Z cross section from CDF of 254.9 ± 16.2 pb [15]. This technique means there is an implicit (small) extrapolation from the measurement range $76 < M_{ll} < 106$ GeV/c^2 presented in this article to the region $66 < M_{ll} < 116$ GeV/c^2, where the inclusive Z cross section measurement was made.

Table III gives the differential results for the ratio of the $Z + b$ jet cross section to the inclusive Z production cross section versus the $E_T^{b\,\mathrm{jet}}$ and $\eta^{b\,\mathrm{jet}}$. These measurements are proportional to the number of b jets. Table IV lists the differential cross section ratios versus p_T^Z, together with the ratio for one and two jets and for one and two b jets. These measurements are proportional to the number of events. Also included in Tables III and IV is the correction factor C_{had} that needs to be applied to parton level calculations to correct for the underlying event and hadronization.

Figs. 4, 5, and 6 show the data compared to the MCFM prediction versus $E_T^{b\,\mathrm{jet}}$ and $\eta^{b\,\mathrm{jet}}$,

TABLE III: The ratio of the $Z + b\,\text{jet}$ to the inclusive Z cross section versus $E_T^{b\,\text{jet}}$ (normalized per GeV) and $\eta^{b\,\text{jet}}$ (normalized per unit in pseudorapidity). The statistical uncertainty is listed first and the systematic uncertainty is listed second. The correction factor C_{had} that needs to be applied to parton level calculations to correct for the underlying event and hadronization is also given.

$E_T^{b\,\text{jet}}$ (GeV)	$\sigma^{\text{jet}}(Z + b\,\text{jet})/\sigma(Z) \times 10^4$ $(\text{GeV})^{-1}$	C_{had}
$[20, 35]$	$1.42 \pm 0.28 \pm 0.15$	1.03
$[35, 55]$	$0.25 \pm 0.10 \pm 0.03$	1.13
$[55, 100]$	$0.122 \pm 0.043 \pm 0.019$	1.22
$\lvert\eta^{b\,\text{jet}}\rvert$	$\sigma^{\text{jet}}(Z + b\,\text{jet})/\sigma(Z) \times 10^3$	C_{had}
$[0.0, 0.5]$	$2.44 \pm 0.57 \pm 0.28$	1.13
$[0.5, 1.0]$	$2.90 \pm 0.65 \pm 0.39$	1.03
$[1.0, 1.5]$	$0.79 \pm 0.50 \pm 0.14$	1.05

versus the number of jets and b jets, and versus p_T^Z, respectively. The MCFM predictions are shown for two different values for the renormalization and factorization scale.

It is seen that the theoretical cross section prediction depends on the choice of scale, and differences up to a factor of two are seen, e.g., in the N_{jet} distribution. Both predictions describe the data but the lower scale choice is favored.

Figs. 7, 8, and 9 show the data compared to the ALPGEN and PYTHIA Monte Carlo programs. Large differences are observed between the two programs, in particular at low $E_T^{b\,\text{jet}}$ and low p_T^Z and at low jet multiplicity. We have verified that this difference is reduced if we use a lower scale for ALPGEN but present here only the default used commonly by hadron collider experiments. In general PYTHIA describes the data better than ALPGEN. Both MC programs describe the data well at high $E_T^{b\,\text{jet}}$ and p_T^Z and for jet multiplicities of two.

All predictions are generally in agreement with the data, but differences of up to 2σ are observed in the integrated cross section between the data and the MCFM calculation, depending on which scale is used. The large spread of the theoretical predictions suggests that higher orders in the QCD calculation may be important for this process.

TABLE IV: The ratio of the $Z + b\,\text{jet}$ to the inclusive Z cross section versus the number of jets, the number of b jets, and the p_T of the Z boson for events with at least one b jet. In all cases the measurement is restricted to $E_T^{b\,\text{jet}} > 20$ GeV and $|\eta^{b\,\text{jet}}| < 1.5$. The statistical uncertainty is listed first and the systematic uncertainty is listed second. The correction factor C_{had} that needs to be applied to parton level calculations to correct for the underlying event and hadronization is also given.

p_T^Z (GeV/c)	$\sigma^{\text{evt}}(Z+ \geq 1b\,\text{jet})/\sigma(Z) \times 10^5$ (GeV/c)$^{-1}$	C_{had}
$[0, 20]$	$4.6 \pm 1.4 \pm 0.7$	1.25
$[20, 35]$	$7.0 \pm 1.9 \pm 0.8$	1.09
$[35, 55]$	$2.9 \pm 1.0 \pm 0.2$	0.93
$[55, 100]$	$1.11 \pm 0.39 \pm 0.15$	1.14
N_{jet}	$\sigma^{\text{evt}}(Z+ \geq 1b\,\text{jet})/\sigma(Z) \times 10^3$	C_{had}
1	$2.23 \pm 0.42 \pm 0.28$	1.07
2	$0.78 \pm 0.22 \pm 0.09$	1.12
$N_{b\,\text{jet}}$	$\sigma^{\text{evt}}(Z + N_{b\,\text{jet}})/\sigma(Z) \times 10^3$	C_{had}
1	$2.75 \pm 0.44 \pm 0.38$	1.07
2	$0.22 \pm 0.11 \pm 0.05$	1.09

X. CONCLUSION

In conclusion, we have measured the ratio of $Z+b\,\text{jet}$ production to inclusive Z production using the CDF II detector at the Tevatron, and compared to previous measurements the uncertainty has been reduced to 20%. For the first time we have presented differential measurements as a function of the kinematics of the jets and Z boson and the number of jets in the event. These measurements enable the NLO QCD prediction to be tested over a wide range of final state observables. Large variations are seen between the theoretical predictions as no full NLO QCD calculation is available for this process. The predictions generally describe the data, but the agreement is better for those predictions that use a low value for the renormalization and factorization scales.

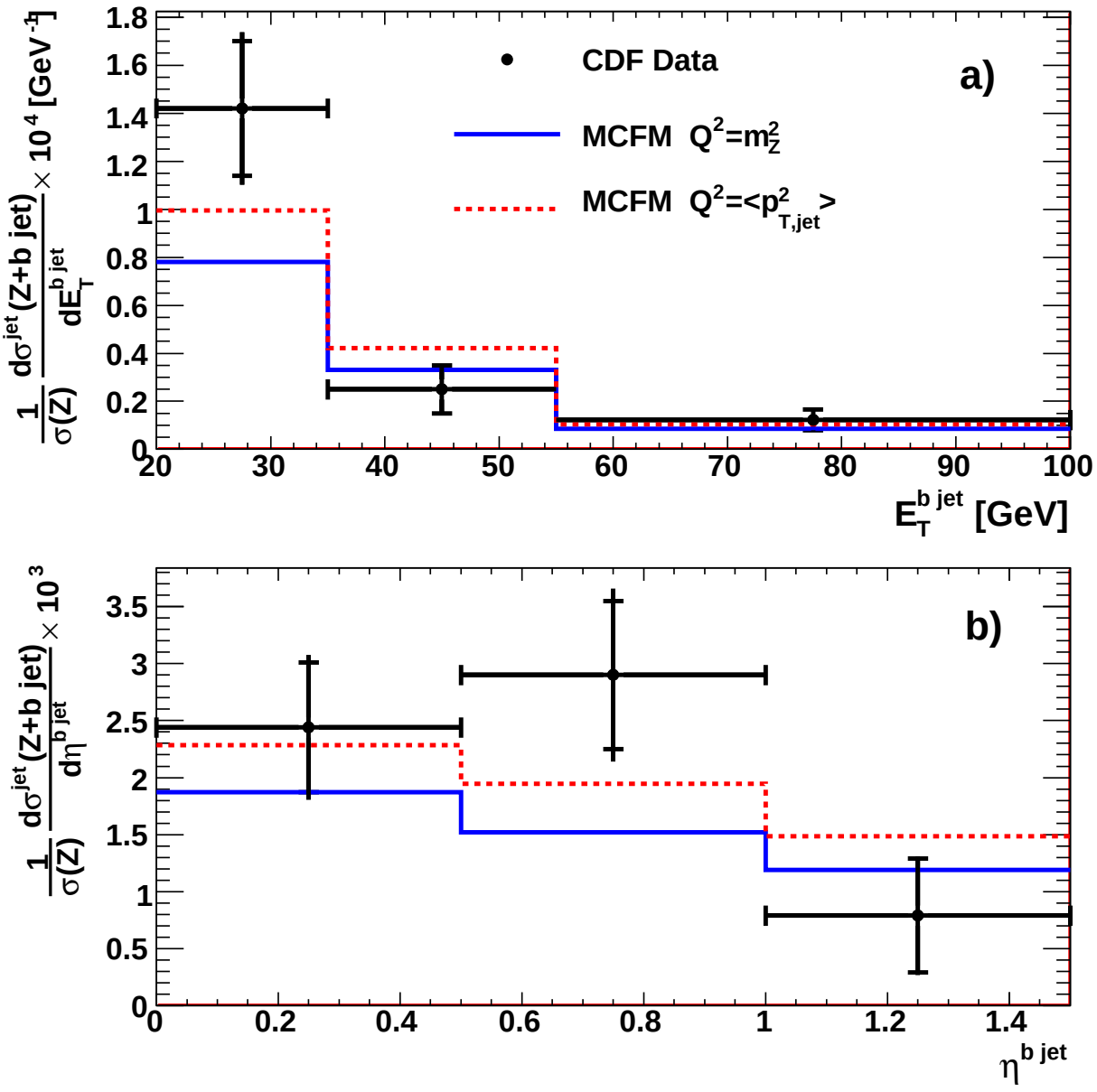

FIG. 4: Ratio of the $Z + b$ jet to the inclusive Z boson cross section versus a) $E_T^{b\,\mathrm{jet}}$ and b) $\eta^{b\,\mathrm{jet}}$. Shown are the data (points) compared to the predictions from MCFM calculated with the scales $Q^2 = m_Z^2 + p_{T,Z}^2$ (solid line) and with $Q^2 = \langle p_{T,\mathrm{jet}}^2 \rangle$ (dotted line). The inner error bars represent the statistical errors, and the outer error bars represent the total errors.

Acknowledgments

We thank the Fermilab staff and the technical staffs of the participating institutions for their vital contributions. We are thankful to J. Campbell, F. Maltoni, M. Mangano, M.

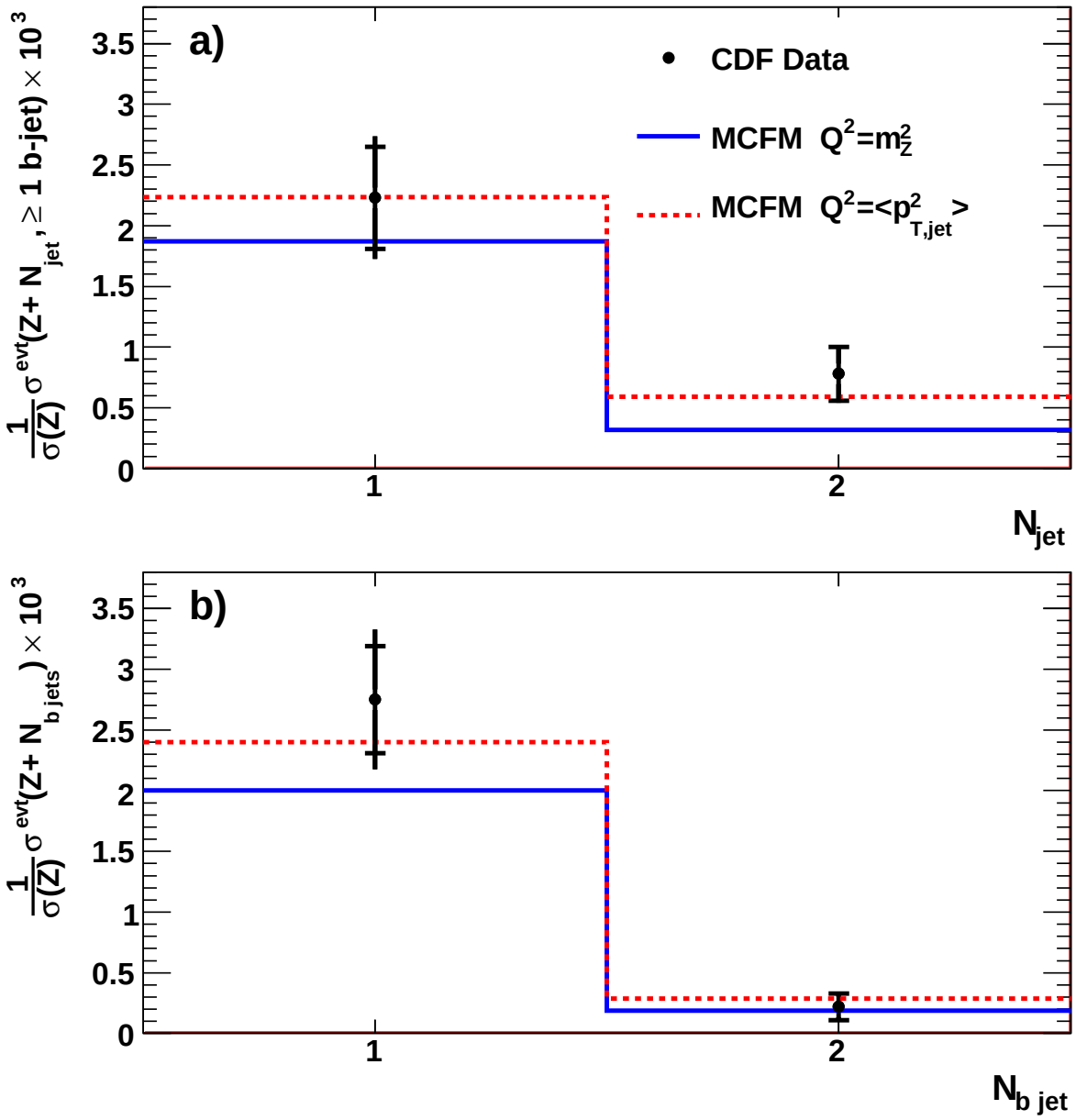

FIG. 5: Ratio of the $Z+b$ jet cross section to the Z boson cross section versus a) $N_{\rm jet}$ and b) $N_{b\,\rm jet}$ .Shown are the data (points) compared to the predictions from MCFM calculated with the scales $Q^2 = m_Z^2 + p_{T,Z}^2$ (solid line) and with $Q^2 = \langle p_{T,\rm jet}^2 \rangle$ (dotted line). The inner error bars represent the statistical errors, and the outer error bars represent the total errors.

Seymour, T. Sjöstrand and J. Thaler for the many interesting and helpful discussions regarding the theoretical predictions. This work was supported by the U.S. Department of Energy and National Science Foundation; the Italian Istituto Nazionale di Fisica Nucleare;

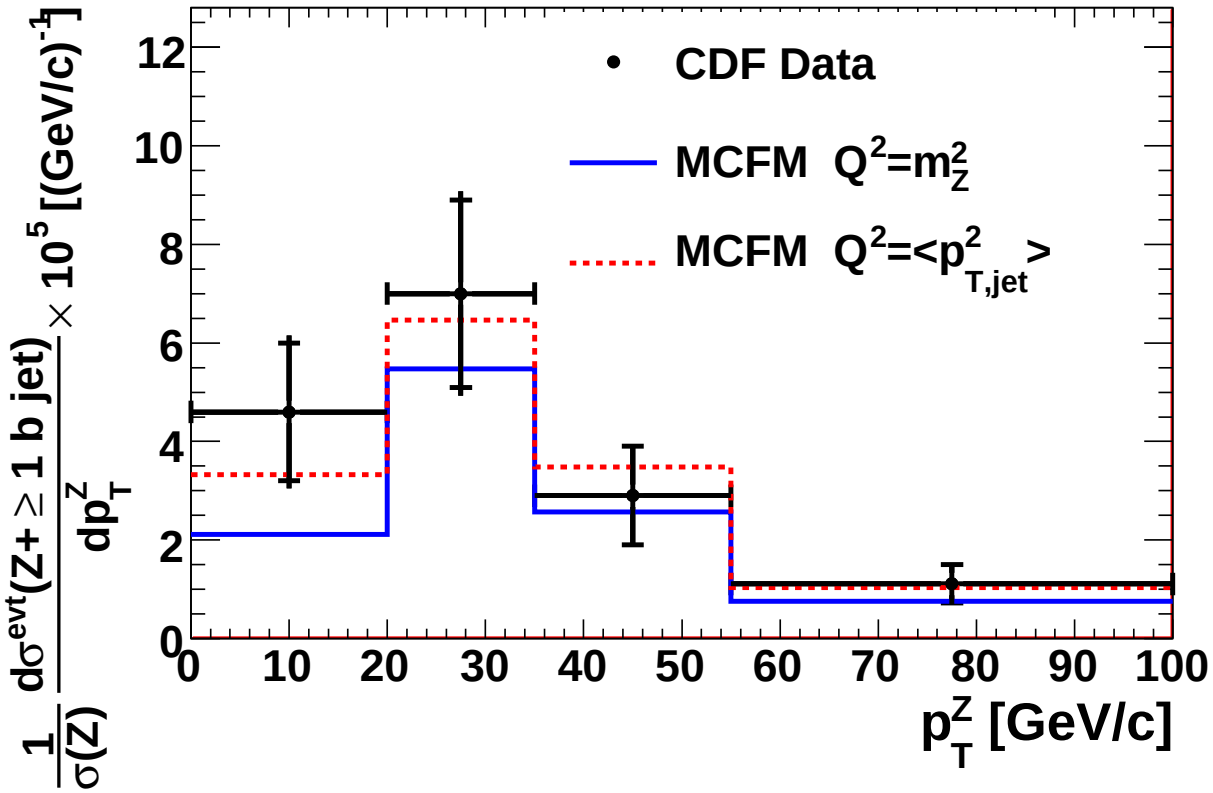

FIG. 6: Ratio of the $Z+b$ jet cross section to the Z boson cross section versus $p_T(Z)$. Shown are the data (points) compared to the predictions from MCFM calculated with the scales $Q^2 = m_Z^2 + p_{T,Z}^2$ (solid line) and $Q^2 = \langle p_{T,\mathrm{jet}}^2 \rangle$ (dotted line). The inner error bars represent the statistical errors, and the outer error bars represent the total errors.

the Ministry of Education, Culture, Sports, Science and Technology of Japan; the Natural Sciences and Engineering Research Council of Canada; the National Science Council of the Republic of China; the Swiss National Science Foundation; the A.P. Sloan Foundation; the Bundesministerium für Bildung und Forschung, Germany; the Korean Science and Engineering Foundation and the Korean Research Foundation; the Science and Technology Facilities Council and the Royal Society, UK; the Institut National de Physique Nucleaire et Physique des Particules/CNRS; the Russian Foundation for Basic Research; the Ministerio de Ciencia e Innovación, and Programa Consolider-Ingenio 2010, Spain; the Slovak R&D Agency; and

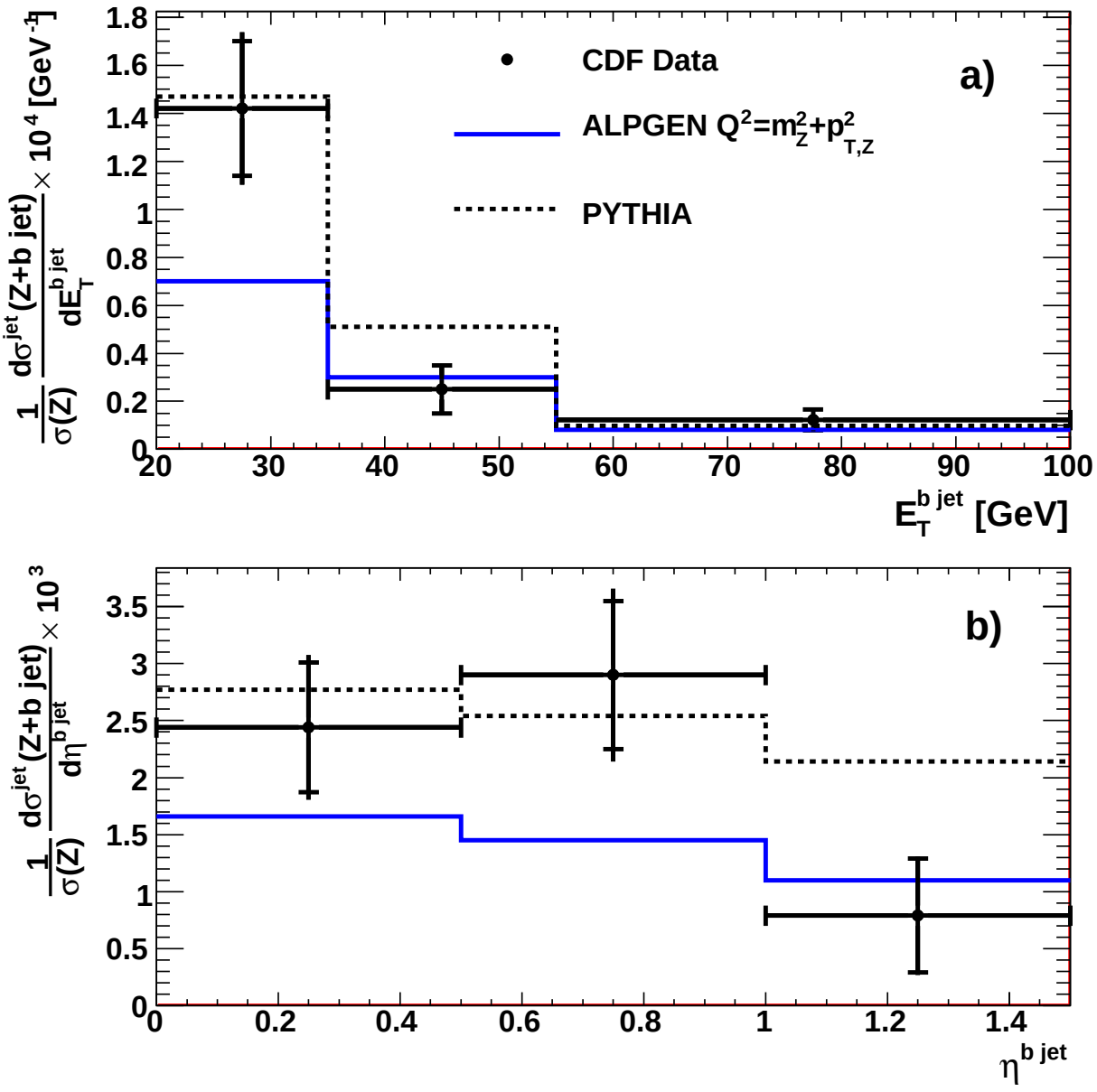

FIG. 7: Ratio of the $Z+b$ jet to the inclusive Z boson cross section versus a) $E_T^{\rm jet}$ and b) $\eta^{\rm jet}$. Shown are the data (points) compared to the predictions from ALPGEN (solid line) and PYTHIA (dotted line). The inner error bars represent the statistical errors, and the outer error bars represent the total errors.

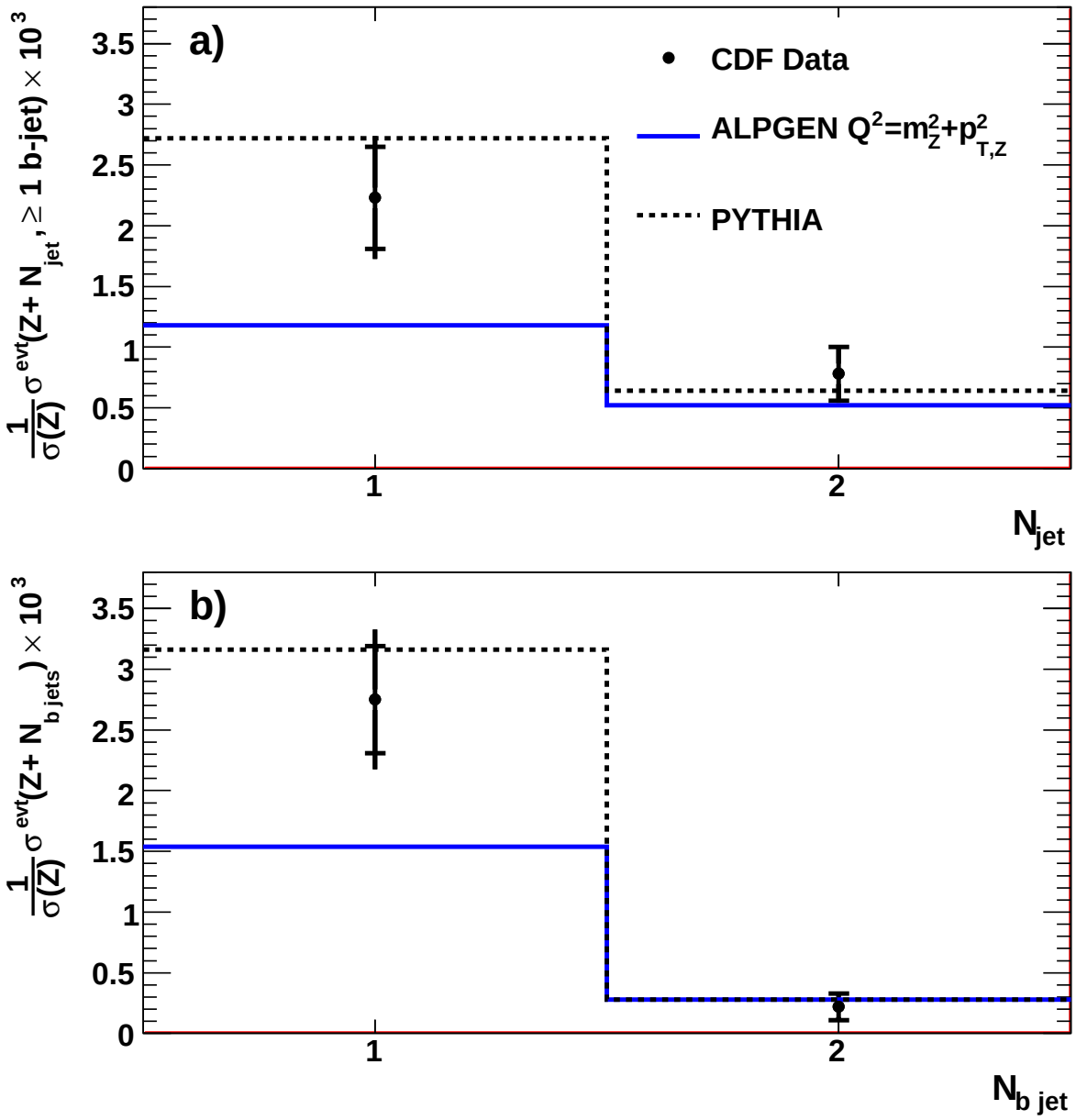

FIG. 8: Ratio of the $Z + b$ jet cross section to the Z boson cross section versus a) $N_{\rm jet}$ and b) $N_{b\,\rm jet}$. Shown are the data (points) compared to the predictions from ALPGEN (solid line) and PYTHIA (dotted line). The inner error bars represent the statistical errors, and the outer error bars represent the total errors.

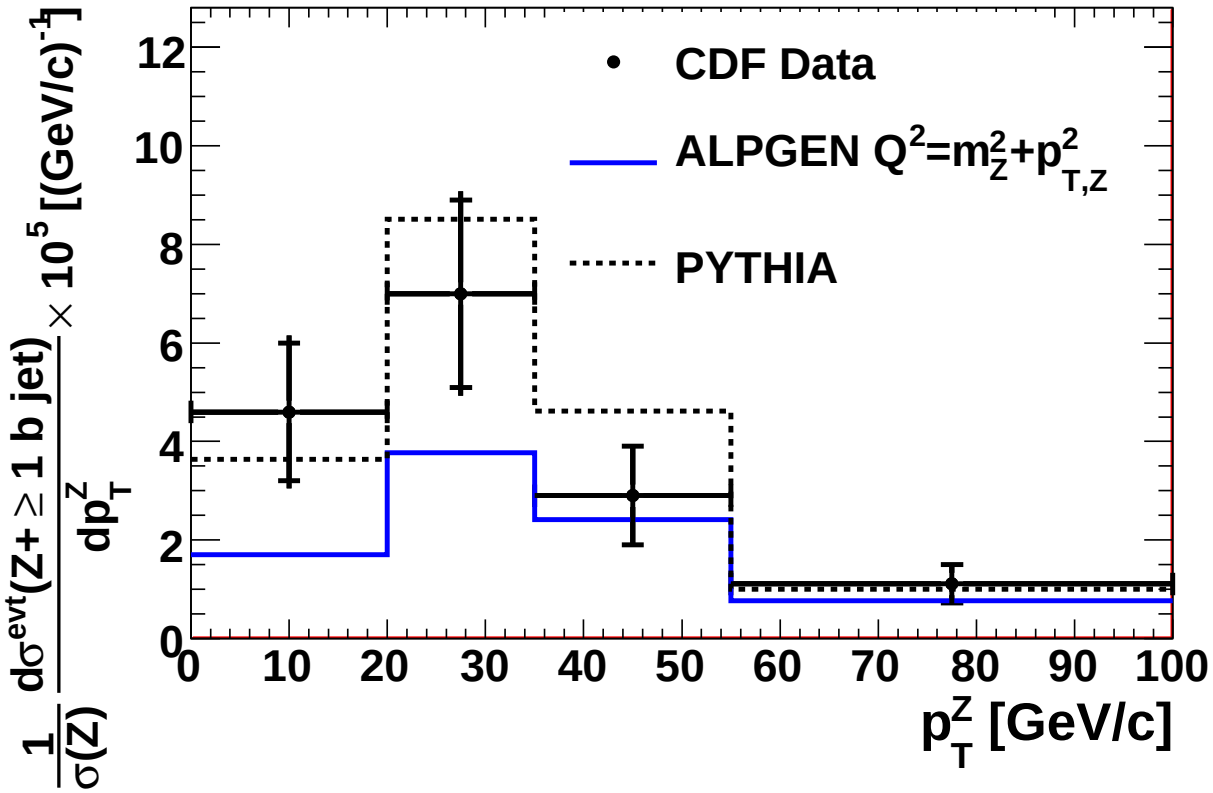

FIG. 9: Ratio of the $Z + b$ jet cross section to the Z boson cross section versus $p_T(Z)$. Shown are the data (points) compared to the predictions from ALPGEN (solid line) and PYTHIA (dotted line). The inner error bars represent the statistical errors, and the outer error bars represent the total errors.

the Academy of Finland.

[1] J. Campbell, R.K. Ellis, F. Maltoni, and S. Willenbrock, Phys. Rev. D **69**, 074021 (2004).

[2] T. Sjöstrand, L. Lönnblad, and S. Mrenna, LU-TP 01, arXiv:hep-ph/0108264.

[3] M. Mangano, M. Moretti, and R. Pittau, Nucl. Phys. B **632**, 343 (2002);
M. Mangano *et al.*, J. High Energy Phys. **0307**, 001 (2003).

[4] M. Carena *et al.*, (Higgs Working Group Collaboration), arXiv:hep-ph/0010338.

[5] V. M. Abazov *et al.* (D0 Collaboration), Phys. Rev. Lett. **97**, 171806 (2006).

[6] T. Aaltonen *et al.* (CDF Collaboration), Phys. Rev. D **76**, 072010 (2007).

[7] T. Stelzer, Z. Sullivan, and S. Willenbrock, Phys. Rev. D **56**, 5919 (1997);
T. Stelzer, Z. Sullivan, and S. Willenbrock, Phys. Rev. D **58**, 094021 (1998).

[8] D. Dicus, T. Stelzer, Z. Sullivan, and S. Willenbrock, Phys. Rev. D **59**, 094016 (1999);
C. Balazs, H. J. He, and C. P. Yuan, Phys. Rev. D **60**, 114001 (1999);
F. Maltoni, Z. Sullivan, and S. Willenbrock, Phys. Rev. D **67**, 093005 (2003).

[9] D. Choudhury, A. Datta, and S. Raychaudhuri, arXiv:hep-ph/9809552;
C. S. Huang and S. H. Zhu, Phys. Rev. D **60**, 075012 (1999);
J. Campbell, R.K. Ellis, F. Maltoni, and S. Willenbrock, Phys. Rev. D **67**, 095002 (2003).

[10] A. Abulencia *et al.* (CDF Collaboration), Phys. Rev. D **74**, 032009 (2006).

[11] V. M. Abazov *et al.* (D0 Collaboration), Phys. Rev. Lett. **94**, 161801 (2005).

[12] T. Aaltonen *et al.* (CDF Collaboration), Phys. Rev. Lett. **100**, 102001 (2008).

[13] V. M. Abazov *et al.* (D0 Collaboration), Phys. Lett. B **658**, 112 (2008).

[14] C. Neu (for the CDF Collaboration), *$W^{\pm}/Z$ + Jets and $W^{\pm}$ / Z + Heavy Flavor Jets at the Tevatron.*, Proceedings of 43rd Rencontres de Moriond on QCD and Hadronic Interactions, La Thuile, Italy, 2008.

[15] A. Abulencia *et al.* (CDF Collaboration), J. Phys. G **34**, 2457 (2007).

[16] D. Acosta *et al.* (CDF Collaboration), Phys. Rev. D **71**, 032001 (2005).

[17] C. S. Hill *et al.*, Nucl. Instrum. Methods A **530**, 1 (2004);
A. Sill *et al.*, Nucl. Instrum. Methods A **447**, 1 (2000);
A. Affolder *et al.*, Nucl. Instrum. Methods A **453**, 84 (2000).

[18] A. Affolder *et al.*, Nucl. Instrum. Methods A **526**, 249 (2004).

[19] L. Balka *et al.*, Nucl. Instrum. Methods A **267**, 272 (1988).

[20] M. Albrow *et al.*, Nucl. Instrum. Methods A **480**, 524 (2002).

[21] S. Bertolucci *et al.*, Nucl. Instrum. Methods A **267**, 301 (1988).

[22] S. Kuhlmann *et al.*, Nucl. Instrum. Methods A **518**, 39 (2004).

[23] G. Ascoli *et al.*, Nucl. Instrum. Methods A **268**, 33 (1988).

[24] D. Acosta *et al.*, Nucl. Instrum. Methods A **461**, 540 (2001).

[25] G. Miu and T. Sjöstrand, Phys. Lett. B **449**, 313 (1999).

[26] M. Mangano *et al.*, J. High Energy Phys. **0701**, 013 (2007).

[27] H.L. Lai *et al.*, Eur. Phys. J. C **12**, 375 (2000).

[28] D. Acosta *et al.* (CDF Collaboration), Phys. Rev. D **70**, 072002 (2004).

[29] R. D. Field (for the CDF Collaboration), *Studying the Underlying Event at CDF*, Proceedings of 33rd International Conference on High Energy Physics (ICHEP 06), Moscow, Russia, 2006.

[30] D. J. Lange, Nucl. Instrum. Methods A **462**, 152 (2001).

[31] GEANT, Detector description and simulation tool, CERN Program Library Long Writeup W5013 (1993).

[32] E. Gerchtein and M. Paulini, *CDF detector simulation framework and performance*, Proceedings of 2003 Conference for Computing in High-Energy and Nuclear Physics (CHEP 03), La Jolla, California, 2003.

[33] D. Acosta *et al.* (CDF Collaboration), Phys. Rev. D **71**, 051103 (2005).

[34] G. Arnison *et al.*, Phys. Lett. B **123**, 115 (1983).

[35] A. Bhatti *et al.*, Nucl. Instrum. Methods A **566**, 375 (2006).

[36] D. Acosta *et al.* (CDF Collaboration), Phys. Rev. D **71**, 052002 (2005).

[37] J. Campbell and R.K. Ellis, Phys. Rev. D **60**, 113006 (1999).

[38] N. Kidonakis and R. Vogt, Eur. Phys. J. C **33**, 466 (2004).

[39] T. Aaltonen *et al.*, (The CDF Collaboration), Phys. Rev. D **77**, 052002 (2008).

[40] S. Klimenko, J. Konigsberg, and T.M. Liss, FERMILAB-FN-0741 (2003).

[41] J. Pumplin *et al.*, J. High Energy Phys. **0207**, 012 (2002);